

## DP590 钢两道次焊接温度场数值模拟与试验验证

邢淑清<sup>1</sup>, 郝 飞<sup>2</sup>, 闫 波<sup>3</sup>, 麻永林<sup>1</sup>

(1. 内蒙古科技大学 材料与冶金学院, 包头 014010;

2. 中石油江苏液化天然气有限公司 检维修中心, 南通 226001;

3. 包头钢铁(集团)公司 技术中心, 包头 014010)

摘 要: 针对汽车用材 DP590 钢, 采用有限元技术, 运用参数化编程语言和生死单元技术, 对该钢的二氧化碳气体保护单面双道焊接进行数值模拟, 并将模拟结果与相同工艺条件下的焊接试验结果比较。结果表明, 用有限元数值模拟方法得到的温度场分布规律与实测温度值基本一致; 后道次的热循环对热影响区的组织有较大影响; 由于再热温度对两道次焊接过程有较大影响, 后道次开始焊接温度控制在 200 ℃ 左右对 DP590 两道次焊接过程比较合理。

关键词: DP590 双相钢; CO<sub>2</sub> 气体保护焊; 数值模拟; 温度场

中图分类号: TG444 文献标识码: A 文章编号: 0253-360X(2012)12-0081-04



邢淑清

## 0 序 言

DP590 钢属于铁素体和马氏体双相钢, 具有较高的强度和优良的塑性, 被世界各国汽车行业一致看好, 应用前景极佳<sup>[1]</sup>。双相(DP)钢的制造和加工技术的研究在国外开始较早, 国内从 1978 年开始对双相钢的变形特征、轧制变形模式、强化原理及断裂特性进行研究, 上海交通大学对双相钢电阻点焊熔核形成过程进行了数值模拟研究, 得到了较好的结果。CO<sub>2</sub> 气体保护焊作为一种高效的焊接方法<sup>[2]</sup>, 以其焊接变形小和焊接成本低的特点, 在国内汽车业得到了广泛的应用。借助有限元软件 ANSYS 对 DP590 钢板的 CO<sub>2</sub> 气体保护焊进行三维数值模拟, 得到焊缝和热影响区的热循环曲线, 分析多道焊焊缝的再加热过程和组织, 结合实测数据, 对模拟结果的可靠性进行验证。研究结果对 DP590 双相钢的焊接工作者有着指导意义。

程是一个加热非常不均匀的过程, 在焊缝处温度梯度变化很大, 划分网格是在焊缝及其附近的部分用加密的网格。单元类型采用具有三个方向热传导能力的 SOLID70 单元。采用自适应映射网格划分技术, 模拟时共生成 19 560 个单元, 22 785 个节点。网格划分如图 1 所示。运用参数化编程语言 APDL 控制计算流程, 将焊缝的单元杀死, 随着焊接的进行, 逐渐激活杀死的单元来实现动态的焊接过程<sup>[3, 4]</sup>。

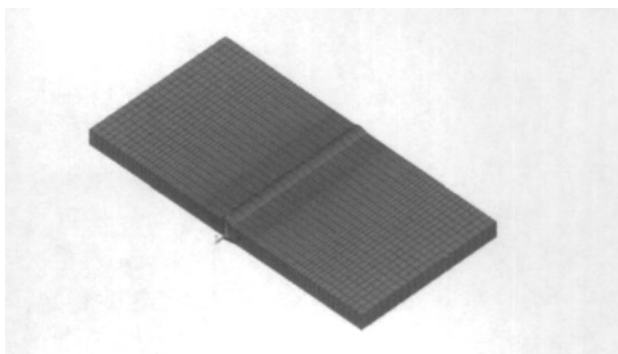


图 1 有限元网格模型

Fig. 1 Model of finite element mesh

## 1 DP590 钢焊接过程有限元分析

## 1.1 建立模型

DP590 钢对接焊, 模型尺寸 100 mm × 100 mm × 7.8 mm, 采用单面 V 形坡口, 坡口角度 60°。焊接过

## 1.2 边界条件和材料热物理性能参数

熔焊时, 由热源传热给焊件的热量主要以辐射和对流为主, 因此在模拟计算中将辐射传热作为对流换热的一部分考虑, 即加大对流系数来实现边界条件的简化。对流换热系数为 10 W/(m<sup>2</sup>·℃)<sup>[5]</sup>, 预热温度 25 ℃。

DP590 钢的主要化学成分为(质量分数): 0.071% C, 0.43% Si, 1.84% Mn, 0.011% P, 0.02% S, 其热物理性能数据见图 2<sup>[6]</sup>, 泊松比取 0.3, 密度取  $7\,826\text{ kg/m}^3$ .

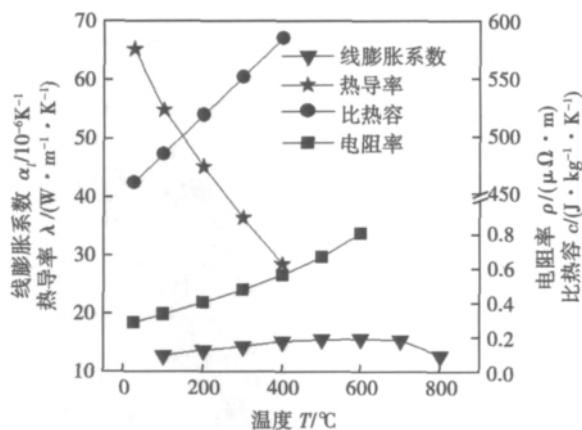


图 2 DP590 钢的热物理性能

Fig. 2 Thermo physical properties parameters of DP590

### 1.3 焊接热输入

采用生热率加载形式, 生热率作为体载荷施加于单元上. 模拟化学反应生热和电流生热. 熔焊时, 由焊接能源输入给单位长度焊缝上的热量称为热输入. 计算公式如下<sup>[7]</sup>, 即

$$Q = nIU/V$$

式中:  $Q$  为单位长度焊缝的热输入 ( $\text{J/m}$ );  $I$  为焊接电流 ( $\text{A}$ );  $U$  为电弧电压 ( $\text{V}$ );  $V$  为一定时间内焊料的体积 ( $\text{m}^3$ );  $n$  为焊接电弧热效率,  $\text{CO}_2$  气体保护焊为  $0.66 \sim 0.69$ .

## 2 温度场模拟结果分析与试验验证

### 2.1 模拟结果分析

采用  $\text{CO}_2$  气体保护单面双道焊, 焊接电流为  $180\text{ A}$ , 电弧电压为  $23\text{ V}$ , 焊接速度  $4\text{ mm/s}$ , 道次间的冷却时间为  $20\text{ s}$ . 在开始时温度场很不稳定, 随着焊接的进行, 焊件温度迅速上升, 经过一段时间后形成稳定的温度场, 热影响区温度显著增加, 温度梯度沿焊缝两侧对称分布, 如图 3a 所示. 第一道次焊接结束后在空气中自然冷却  $20\text{ s}$ , 图 3b 所示为空冷  $20\text{ s}$  时的温度场, 可以看出此时最高温度为  $454\text{ }^\circ\text{C}$ , 焊件边缘处温度仍接近室温, 焊接开始处的温度已经降到  $230\text{ }^\circ\text{C}$  左右. 再进行第二道次焊接, 由于第一道次的预热作用, 使得第二道次的初始温度较第一道次初始温度有明显的升高, 当焊接到  $57.5\text{ s}$  时的温度场如图 3c 所示. 第  $70\text{ s}$  焊接结束, 在空气中

冷却至室温, 图 3d 所示为冷却到  $180\text{ s}$  时的温度场.

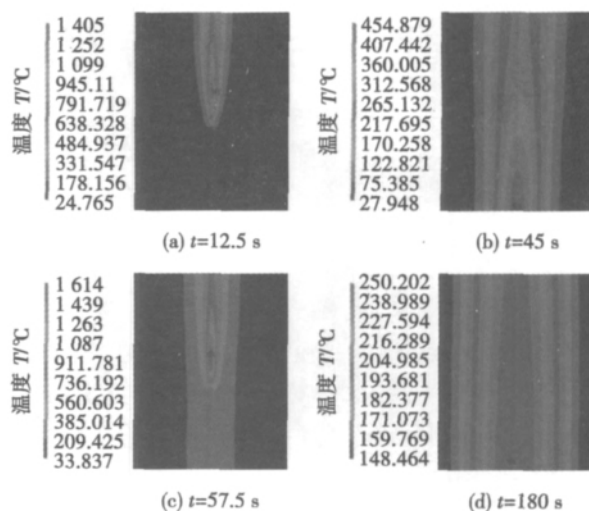


图 3 焊接接头温度分布

Fig. 3 Temperature distribution of welded joints

如图 4 所示, 在  $z = -50\text{ mm}$ ,  $y = 0\text{ mm}$  处的焊缝中心取点 1, 之后每隔  $4\text{ mm}$  取一点, 依次取 1, 2, 3, 4, 5 五个点. 在 ANSYS 中绘制出这 5 个点的温度随时间变化历程曲线(图 5).

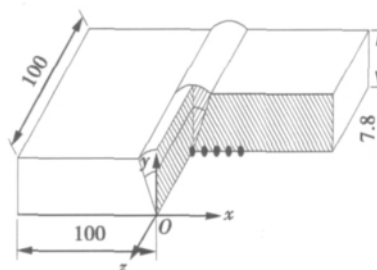


图 4 焊缝取点示意图 (mm)

Fig. 4 Schematic diagram of weld access point

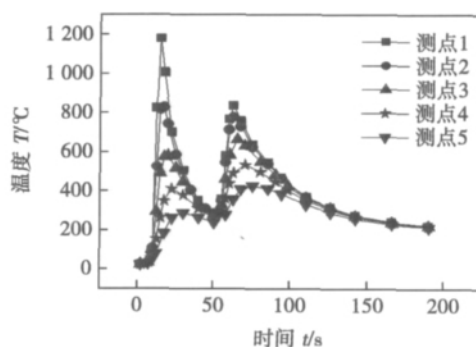


图 5 各点温度变化历程

Fig. 5 Temperature history diagram of measuring points

由图 5 可知在每一道焊接过程中, 测点的温度

随着焊接热源的接近和离去而迅速上升和下降,其温度循环特征相似;当焊接热源移动到该截面时,该截面的温度急剧上升,测点最高温度 1 230 ℃,热源移动过后温度迅速下降,且随离焊缝渐远,峰值温度越低;由于后道焊接对焊缝及热影响区有再热作用,且高温持续时间较长,测点 1 再热的  $t_{8/5}$  为 36 s,后道焊接的再热温度对焊缝及 HAZ 的组织有较大影响。

焊缝的显微组织如图 6 所示。采用 CO<sub>2</sub> 气体保护焊,焊缝组织基本是细小、均匀的针状铁素体 + 少量的珠光体(图 6a)。经过再热后的焊缝中先共析铁素体沿柱状晶晶界分布,少量无碳贝氏体由晶界向晶内平行生长,晶内为粒状贝氏体、索氏体和大量相互穿插的针状铁素体,然后富碳的奥氏体转变为珠光体(图 6b)。

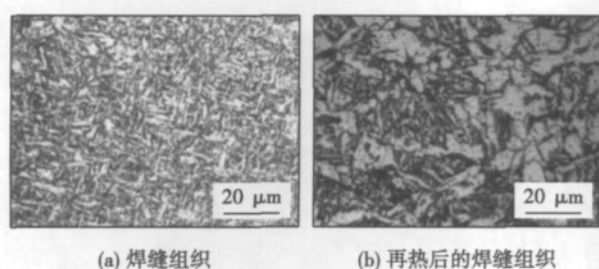


图 6 焊缝显微组织

Fig. 6 Microstructure of welding seam

## 2.2 接头硬度

针对组织的变化对工件接头质量的影响,测量了 DP590 钢两道次焊接后的显微硬度,如图 7 所示。可以看出,CO<sub>2</sub> 焊试件的接头显微硬度整体水平较高,从焊缝中心到热影响区显微硬度逐渐在升高,且在焊缝和热影响区交界部分显微硬度达到峰值,焊接接头的硬度值分布情况一般是熔合线及其附近硬度值最高,距熔合线越远,硬度值逐渐下降,直到接近母材。

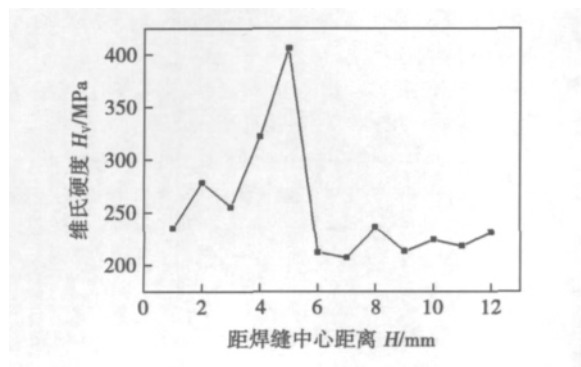


图 7 硬度曲线

Fig. 7 Hardness curve

## 2.3 冷却时间对再热温度的影响

在热输入一定的情况下,调整道次间的冷却时间是有效的控制预热温度的方法。为此模拟在冷却时间为 10 ~ 90 s 条件下,测点 1 的再热循环曲线如图 8 所示。比较图 8 中的结果可以看出随着冷却时间加长,最低温度和再热最高温度都有所下降,且冷却速度与时间成反比。

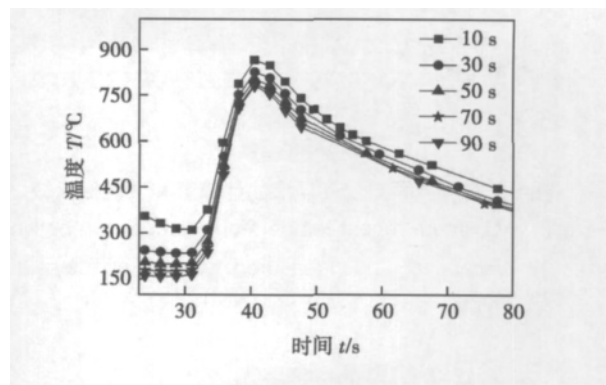


图 8 再热循环曲线

Fig. 8 Reheat cycle curve

从模拟结果可得表 1 的参数,可以发现最高温度降低数值超过最低温度降低数值的一半,高温持续时间随最低温度的降低也明显的缩短。在 50 s 后,即冷却至 200 ℃后,最高温度和高温持续时间的减小速率明显降低,所以从工作效率考虑,在能够满足质量要求的前提下,DP590 钢的 CO<sub>2</sub> 气体保护焊的道次间冷却温度不宜低于 200 ℃。

表 1 不同冷却时间的再热循环特征参数

Table 1 Characteristic parameters of reheat cycle with different cooling time

冷却时间 $t/s$	最低温度 $T_{\min}/^{\circ}\text{C}$	最高温度 $T_{\max}/^{\circ}\text{C}$	高温停留时间 $> T_{500}/s$
10	312	867	35.8
30	235	828	31.5
50	201	806	29
70	177	800	27.6
90	161	783	26.7

## 2.4 试验验证与误差分析

为了检验模拟计算结果,进行了相同焊接工艺的焊接试验,试验中利用热电偶、XSR30 无纸记录仪和计算机系统对焊接过程中测点的热循环进行测定、记录和显示。

在试验中两道次共用 74 s。一道次焊接用 23 s,中间冷却 20 s,二道次焊接用 31 s。当焊接进行到 62.5 s 时,测点 1 的再热温度达到最高的 843 ℃,对

比各测点的最高再热温度的计算值和试验测定值,如图 9 所示。

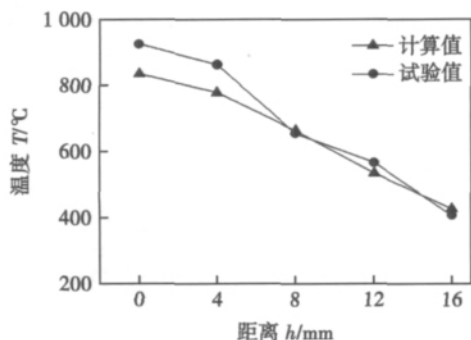


图 9 各测点再热最高温度的计算值和试验值比较

Fig. 9 Maximum reheating temperature comparison between calculated and measured values of measuring points

通过定量比较可以看出,在  $x$  方向上的 1~5 测点仿真得到的温度和试验测得的温度比较接近,仿真温度略低于试验温度,通过分析最大误差不超过 10%。图 10 为第 1 测点在整个焊接过程中,温度随时间变化 ( $T-t$ ) 的计算模拟值与试验测定值的比较。由图 10 可以看出计算值与试验值基本吻合。综上所述,通过计算机模拟计算得到的温度场和实际焊接的温度场有较高的相似度,二者温度场分布情况吻合较好,这样的模拟方法可行。

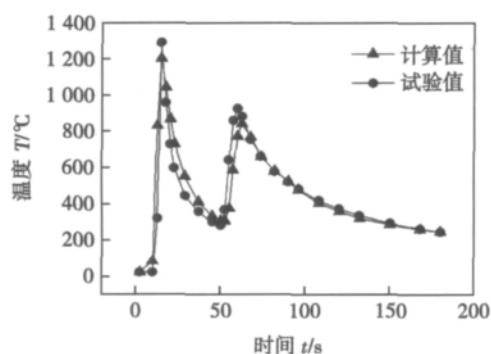


图 10 测点 1 热循环曲线对比

Fig. 10 Thermal cycle curve comparison of No. 1

### 3 结 论

(1) 在两道次焊接过程中,后道次焊接对焊缝及热影响区的再加热过程及其组织有较大影响,焊缝组织基本是细小、均匀的针状铁素体+少量的珠光体,经过再热后的焊缝为先共析铁素体沿柱状晶晶界分布,少量无碳贝氏体由晶界向晶粒内平行生

长,晶粒内为粒状贝氏体、索氏体和大量相互穿插的针状铁素体。

(2) 道次间冷却温度对再热最高温度和高温持续时间有很大影响,DP590 钢的  $CO_2$  气体保护焊道次间温度不宜低于 200  $^\circ C$ 。

(3) 通过模型再现焊接过程,与试验结果的对比及误差分析,表明二者温度场分布情况吻合较好,误差小于 10%,说明该模拟计算方法可行。

### 参考文献:

- [1] 叶平,沈剑平,王光耀,等. 汽车轻量化用高强度钢现状及其发展趋势[J]. 机械工程材料,2006,30(3): 4-7.  
Ye Ping, Shen Jianping, Wang Guangyao, et al. Current status and development of light-weighting high strength steel used in automobiles [J]. Materials for Mechanical Engineering, 2006, 30(3): 4-7.
- [2] 江淑园,郑晓芳,陈焕明,等. 外加磁场对  $CO_2$  焊飞溅的控制机理[J]. 焊接学报,2004,25(3): 65-67.  
Jiang Shuyuan, Zheng Xiaofang, Chen Huanming, et al. Outside magnetic field control to spatter of  $CO_2$  arc welding [J]. Transactions of the China Welding Institution, 2004, 25(3): 65-67.
- [3] 赵洪运,舒凤远,张洪涛,等. 基于生死单元的激光熔覆温度场数值模拟[J]. 焊接学报,2010,31(5): 81-84.  
Zhao Hongyun, Shu Fengyuan, Zhang Hongtao, et al. Numerical simulation on temperature field of laser cladding based on birth-death element method [J]. Transactions of the China Welding Institution, 2010, 31(5): 81-84.
- [4] 孟庆国,方洪渊,徐文立,等. 考虑金属逐步填充的多道焊温度场数值模拟[J]. 焊接学报,2004,25(5): 53-59.  
Meng Qingguo, Fang Hongyuan, Xu Wenli, et al. Numerical simulation of multi-pass welding temperature field taking account of metal filling [J]. Transactions of the China Welding Institution, 2004, 25(5): 53-59.
- [5] 谢元峰. 基于 ANSYS 的焊接温度场和应力的数值模拟研究[D]. 武汉: 武汉理工大学,2006.
- [6] 王敏,张海涛,潘华,等. DP590 双相钢电阻点焊熔核形成过程的数值模拟[J]. 上海交通大学学报,2009,43(1): 56-60.  
Wang Min, Zhang Haitao, Pan Hua, et al. Numerical simulation of nugget formation in resistance spot welding of DP590 dual-phase steel [J]. Journal of Shanghai Jiaotong University, 2009, 43(1): 56-60.
- [7] 张建强,赵海燕,吴甦,等. 焊接电弧热效率的力学测试方法[J]. 焊接学报,2003,24(6): 63-65.  
Zhang Jianqiang, Zhao Haiyan, Wu Su, et al. Mechanical measuring and calculation method of heat efficiency of welding arc [J]. Transactions of the China Welding Institution, 2003, 24(6): 63-65.

作者简介: 邢淑清,女,1971 年出生,硕士,教授,硕士研究生导师。主要从事材料加工、数值模拟及组织性能控制方面的科研和教学工作。发表论文 30 余篇。Email: xingshuqing@imust.cn  
通讯作者: 麻永林,男,教授。Email: malin@imust.cn

### A GABP optimized algorithm for filler rate of non-heated wire

ZHANG Pengxian<sup>1,2</sup>, LI Hao<sup>1,2</sup>, ZHANG Jie<sup>1</sup> (1. Key Laboratory of Non-ferrous Metal Alloys, The Ministry of Education, Lanzhou University of Technology, Lanzhou 730050, China; 2. State Key Laboratory of Gansu Advanced Non-ferrous Metal Materials, Lanzhou University of Technology, Lanzhou 730050, China). pp 77–80

**Abstract:** For the process of submerged arc welding filled with non-heated wire, the filler quantity of non-heated wire is one of the main parameters that affects the microstructure and mechanical properties of welded joints. First, through a lot of welding experiment, the effect of the filler quantity of non-heated wire on the microstructure and mechanical properties was investigated. On the basis of the heat balance law in welding process, the balance equation of heat dynamic distribution for the process of submerged arc welding filled with non-heated wire was established. Then the relational expression was formulated for the filler rate of non-heated wire. At last, the nonlinear mapping relationship between the welding current  $I$ , arc voltage  $U$ , welding speed  $v$  and filler rate of non-heated wire  $vl$  was realized based on artificial neural network. Experimental results showed that, the optimized algorithm of BP neural network based on genetic algorithm (GABP) can realize adaptive control for the process of submerged arc welding filled with non-heated wire. The linear correlation between filler rate of non-heated wire in actual welding process and the expectative output comes up to 0.991 88. This shows that the algorithm of GABP can meet requirement for welding process and properties.

**Key words:** submerged arc welding filled with non-heated wire; heat dynamic distribution; genetic algorithm; BP neural network

### Simulation and experimental verification of double-pass welding temperature field for DP590 steel

XING Shu-qing<sup>1</sup>, HAO Fei<sup>2</sup>, YAN Bo<sup>3</sup>, MA Yonglin<sup>1</sup> (1. School of Material and Metallurgy, Inner Mongolia University of Science and Technology, Baotou 014010, China; 2. Inspection and Maintenance Center, PetroChina LNG Jiangsu Co., Ltd, Nantong 226400, China; 3. Technology Center, Baotou Iron and Steel Co., Ltd, Baotou 014010, China). pp 81–84

**Abstract:** DP590 steel has been widely applied in the field of automobile industry. In present paper, the double-pass welding process in single-sided of CO<sub>2</sub> gas shielding was simulated by using parametric programming language and life-and-death cell technology. The numerical simulation results were compared with the experimental results obtained with the same preconditions. The results showed that the simulation result of temperature distribution within the sample is generally consistent with the measured temperature value. Compared with that of the first welding pass, the thermal cycling of the second pass has a greater impact on microstructure across the heat-affected zone. Because of the great influence of reheating temperature on the multi-pass welding process, it will be more advisable to maintain the temperature of the steel at around 200 °C at the beginning of second welding pass.

**Key words:** DP590 dual-phase steel; CO<sub>2</sub> gas shielded welding; numerical simulation; temperature field

### Optimum design of magnesium alloy welding parameters with GTAW under magnetic field

SU Yunhai, JIANG Huanwen, WU Deguang, LIU Zhengjun (School of Material Science and Engineering, Shenyang University of Technology, Shenyang 110870, China). pp 85–88

**Abstract:** During the welding of AZ31 magnesium alloy plate by GTAW, AC longitudinal and conversion magnetic field were used. The magnetic field current and magnetic field frequency can be adjusted during welding process. Orthogonal experimental design was used to study the effect of parameters on the properties and microstructure of welded joint. The properties of tensile strength and hardness of welded joint were tested. The microstructure of magnesium welded joint was analyzed by metallographic microscope at the same time. The results show that the optimal properties of magnesium alloy welded joint are obtained when welding current is 80 A, magnetic field current is 2 A, and frequency is 20 Hz.

**Key words:** magnesium alloy; welding process under magnetic field; parameters optimum design

### Factors affecting deformation induced martensitic transformation of SUS304 stainless steel

YANG Jianguo<sup>1,2</sup>, CHEN Shuangjian<sup>1,3</sup>, HUANG Nan<sup>1</sup>, FANG Kun<sup>1</sup>, YUAN Shijian<sup>1</sup>, LIU Gang<sup>1</sup>, HAN Cong<sup>5</sup> (1. State Key Laboratory of Advanced Welding and Joining, Harbin Institute of Technology, Harbin 150001, China; 2. Institute of Process Equipment and Control Engineering, Zhejiang University of Technology, Hangzhou 310032, China; 3. Shanghai Institute of Applied Physics, Shanghai 201800, China). pp 89–92

**Abstract:** Tensile tests of SUS304 stainless steel specimens were performed with different strain rates at different temperatures. Moreover, the martensite induced by deformation was analyzed by ferrite measuring instrument, optical microscopy and XRD. Experimental results show that the transformation of martensite is closely related to uniformity of microstructure, strain rate and temperature. At room temperature, the amount of martensite induced by deformation increases with the increasing of tensile strain. For the tailor-welded tube endured 30% circumference strain in hydroforming process at temperature, the amount of martensite is higher in fusion zone than that in HAZ, and it is fewer in the base metal, i. e., the higher the uniformity, the less the amount of martensite transformation induced by deformation from austenite. The amount of martensite decreases with the increasing of testing temperature. Tensile tests at 275 °C indicated that martensite transformation induced by deformation can be restrained in the process of plastic deformation at this temperature, the volume fraction of martensite is almost 0 under such conditions.

**Key words:** deformation induced martensitic transformation; strain rate; microstructure heterogeneity; temperature; influencing factor

### Forming process study of friction stir welding joint

ZHAO Huaxia, DONG Chunlin, LUAN Guohong (Beijing Aeronautical Manufacturing Technology Research Institute, Aviation Industry Corporation of China, Beijing 100024, China). pp 93–96